HiSST: 2nd International Conference on
High-Speed Vehicle Science Technology
11–15 September 2022, Bruges, Belgium

Nonlinear Aeroelastic Behaviors of Cylindrical Composite Skin of a Rocket

Xiaomin An[1], Bin Deng[2]

Abstract

Nonlinear aeroelastic behaviours of three cylindrical composite panels of a rocket skin, which have two different curvatures as R=2.5 and R=5, as well as two layer orientations, cross-ply and angle-ply are studied in a low supersonic flow. The finite element co-rotational theory is applied to model geometrically nonlinear shell panels, and an Euler solver, instead of piston theory or other simplified aerodynamic theories, is utilized to solve unsteady aerodynamic. A fluid-structure staggered coupling program is applied to simulate the nonlinear response. The results, static aeroelastic deformation, limit cycle oscillations and non-periodic oscillations behaviours have been obtained. Flutter dynamic pressure, amplitudes and spectra of limit cycle oscillations are analysed.

Keywords: *static deformation, nonlinear aeroelasticity, composite structure, flutter onset.*

Nomenclature

Latin
E – Elastic modulus
G – Shear modulus
$\boldsymbol{K}_{T,n}$ – Tangent stiffness matrix
$\boldsymbol{M}$ – Global mass matrix
$\boldsymbol{F}_{i,n}$ – Global internal force vector
$\boldsymbol{F}_{s,n+1}$ – Unsteady aerodynamic load
$\bar{\boldsymbol{U}}$ – fluid variables
$\bar{\boldsymbol{Q}}$ – Inviscid flux
$\boldsymbol{d}_n$ – Displacement vector
$\dot{\boldsymbol{d}}_n$ – Velocity vector
$\ddot{\boldsymbol{d}}_n$ – Acceleration vector
$\Delta\boldsymbol{d}$ – Displacement increment vector
t – Real-time of the fluid sover
R – radius
Ma – Mach number
Greek
Ω – Moving control finite volume
τ – Pseudo time the fluid sover
λ – Non-dimensional dynamic pressure
ρ_s – The density of the skin
μ_{12} – Poisson's ratio
Subscripts
i – Inner
n – Step number
a – Aerodynamic domain
s – Structural domain

1. Introduction

In modern aerospace industry, the exposed skin of the rocket always has a certain curvature and consists of composite materials. Consequently, the static aeroelastic deformation will arise and the aeroelastic behaviours will present a more complex characteristic under unsteady aerodynamic loading. The complexity of aeroelastic problem arises from the added difficulties associated not only from the curvature, but also material nonlinear effects. Some researchers have focused their study on the aeroelastic characteristic of the composite panel in supersonic flow, Shiau and Lu [1] investigated the nonlinear flutter behaviors of a composite laminated plate at high supersonic Mach number. The results showed that the anisotropic properties have significant effects on the aeroelastic behaviour. Ganapathi et al. [2] modeled an orthotropic and laminated anisotropic circular cylindrical shell in supersonic flow

[1] *School of Astronautics, Northwestern Polytechnical University, Xi'an, 710072, China. E-mail: frank805@nwpu.edu.cn*
[2] *School of Astronautics, Northwestern Polytechnical University, Xi'an, 710072, China. E-mail: deng2@mail.nwpu.edu.cn*

using finite element based on the field-consistency approach and studied the effects of aspect ratio, thickness, internal pressure, the number of layers and lamination scheme on the flutter boundaries. Singha and Mandal [3] used the isoparametric degenerated shell element and a linear potential flow theory for solving the effects of curvature, laminate stacking sequence and air flow direction on the supersonic flutter characteristics of laminated composite cylindrical panels. Castro et al. [4] presented a modified piston theory to predict the aeroelastic response of laminated composite stiffened panels, and the results showed that the stiffener base significantly affects the panel aeroelastic behavior.

To the best of the authors' knowledge, there are few published works on the nonlinear aeroelastic behaviours of cylindrical composite panels in low supersonic flow regime. The nonlinearity, arising from curvature effect, material property and shock wave movement has not been thoroughly understood. This paper will do some research for simulating nonlinear aeroelastic behaviours of cylindrical composite skins in a low supersonic flow.

2. Cylindrical composite skin's model and calculating procedure

2.1. Cylindrical composite skin's model

The cylindrical structure of a clamped rocket skin is shown in Fig. 1. The curvature of the panel is set as R=5m and R=2.5m. Five equal thickness layers, which have cross-ply and angle-ply are considered. The structural properties are: $a = b = 1.0m$, E_1=40Gpa, E_2=1Gpa, G_{12}=0.6Gpa, G_{13}=0.5Gpa, $\mu_{12} = 0.25$ and $\rho_s = 1500\mathrm{kg}/m^3$. The total thickness of the skin is given as $h = 0.005m$. The structure is discretized by triangular shell element in the co-rotational local coordinate system, and the stress-strain relations of composite layer described in the laminate coordinate system are transformed into the local frame, then, via virtual work and Hamilton's formulation, the nonlinear governing equation of the cylindrical shell can be obtained.

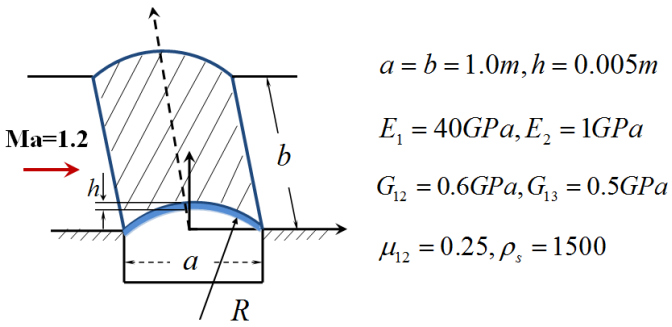

Fig. 1 Geometry of a cylindrical composite skin

In the present study, the nonlinear aeroelastic responses of three cylindrical composite skin with different curvature and orientation of plies are calculated (shown in Table1). 1) R=5m with cross-ply [0°/90°/0°/90°/0°]; 2) R=2.5m with cross-ply [0°/90°/0°/90°/0°]; and 3) R=2.5m with angle-ply [45°/-45°/45°/-45°/45°].

Table 1. Three cylindrical composite panels of the skin

Case	*R*	Orientation of plies	Mach Number
1	5m	[0°/90°/0°/90°/0°]	1.2
2	2.5m	[0°/90°/0°/90°/0°]	1.2
3	2.5m	[45°/-45°/45°/-45°/45°]	1.2

2.2. Staggered coupling Procedure

The nonlinear aeroelastic responses are calculated by Farhat's second-order loosely coupling procedure. Following are details about the major steps of the coupled procedure:

STEP 1: Predict the structural displacement at time-step $n + 1/2$ by the structural motion at n step, and transfer the predicted motion to the fluid system as $\boldsymbol{x}_{n+1/2}$, that is

$$\boldsymbol{x}_{n+1/2} = \boldsymbol{d}_n + \dot{\boldsymbol{d}}_n \Delta t/2 \tag{1}$$

Where $\boldsymbol{d}_n$ and $\dot{\boldsymbol{d}}_n$ are the vectors of the displacement and velocity, respectively; Δt is the time-step.

STEP 2: Update the position of the fluid grids by moving-grid technique.

STEP 3: An AUSMpw+ scheme is utilized to discretize the inviscid flux, and an implicit course of the dual-time technology [5] is introduced to solve the Euler equation to obtain unsteady aerodynamic load $\boldsymbol{F}_{a,n+1/2}$.

$$\Omega \frac{d\bar{U}}{d\tau} + \frac{3\Omega_{n+1/2}\bar{U}_{n+1/2} - 4\Omega_{n-1/2}\bar{U}_{n-1/2} + \Omega_{n-3/2}\bar{U}_{n-3/2}}{2dt} + \bar{\boldsymbol{Q}}_{n+1/2} = \boldsymbol{0} \tag{2}$$

Where Ω is the moving control finite volume. $\bar{\boldsymbol{U}}$ is the vector of the fluid variables , $\bar{\boldsymbol{Q}}$ is inviscid flux and can be obtained by the upwind flux splitting scheme. τ and t are pseudo and real-time, respectively.

STEP 4: Convert the aerodynamic loads $\boldsymbol{F}_{a,n+1/2}$ into structure element as$\boldsymbol{F}_{s,n+1/2}$, and compute the equivalent loads by

$$\boldsymbol{F}_{s,n+1} = 2\boldsymbol{F}_{s,n+1/2} - \boldsymbol{F}_{s,n} \tag{3}$$

STEP 5: Solve nonlinear governing equation of the cylindrical skin by Newmark algorithm to get the structural motion at time-step $n+1$.

$$\boldsymbol{M}\ddot{\boldsymbol{d}}_{n+1} + \boldsymbol{K}_{T,n}\Delta\boldsymbol{d} = \boldsymbol{F}_{s,n+1} - \boldsymbol{F}_{i,n} \tag{4}$$

Where $\boldsymbol{M}$ is the global mass matrix, $\boldsymbol{F}_{i,n}$ and $\boldsymbol{F}_{s,n+1}$ are the global inner force and unsteady aerodynamic load, respectively. $\Delta\boldsymbol{d}$ and $\ddot{\boldsymbol{d}}_{n+1}$ are the vectors of the displacement increment and acceleration, respectively.

For each case, the steady rigid panel solution is computed firstly, and then a disturbance velocity is applied to the panel at the initial time of the coupled procedure under different dynamic pressure.

3. Results and Discussion

Firstly, the static aeroelastic deformations are analyzed for three cases under several non-dimensional dynamic pressure λ. Fig. 2 shows the static deflection versus dynamic pressure. It is observed that the negative deflections at the reference point of the ply [45°/-45°/45°/-45°/45°] are much larger than those of [0°/90°/0°/90°/0°] cases with the increase of dynamic pressure. Figure 3-5 show the Mach number distribution at the section y/b=0.5 and displacement distribution in the z-direction on the surface of the panel at λ=226 for the three cases, respectively. There are oblique shock wave and expansion wave on the leading and tailing edge of the panel. Due to the larger curvature, a bow shock wave, following by a subsonic region, occurs close to the leading edge as shown in Fig. 4(a) and Fig. 5(a). The displacements distribution of the two panels with ply [0°/90°/0°/90°/0°] have the same pattern as the panel moves downwards at the front part whereas it travels upwards at the back part along the flow direction. Nevertheless, the [45°/-45°/45°/-45°/45°] panel has only one negative peak.

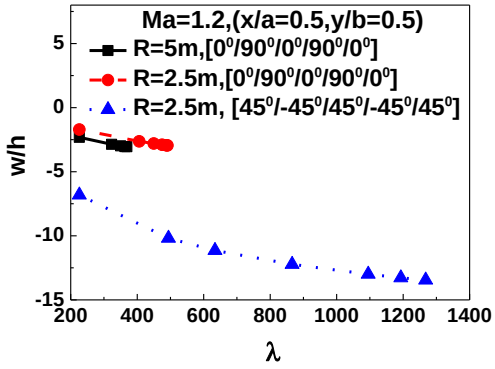

Fig. 2 Static deflection vs. dynamic pressure

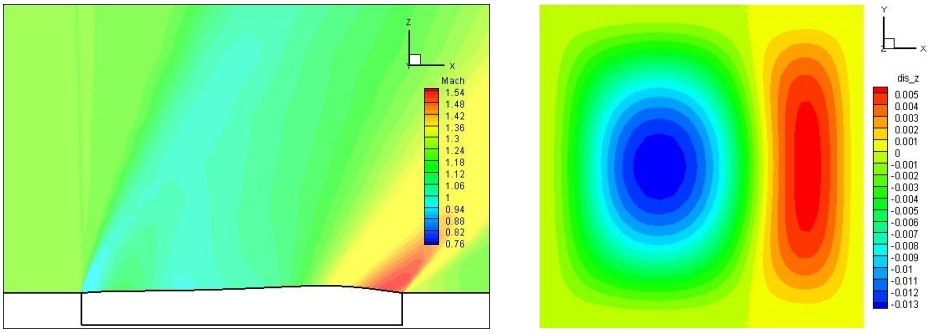

(a) Mach number distribution at the section y/b=0.5; (b) Displacement distribution of the panel

Fig. 3 Mach number and displacement distribution at λ=226 for Case 1

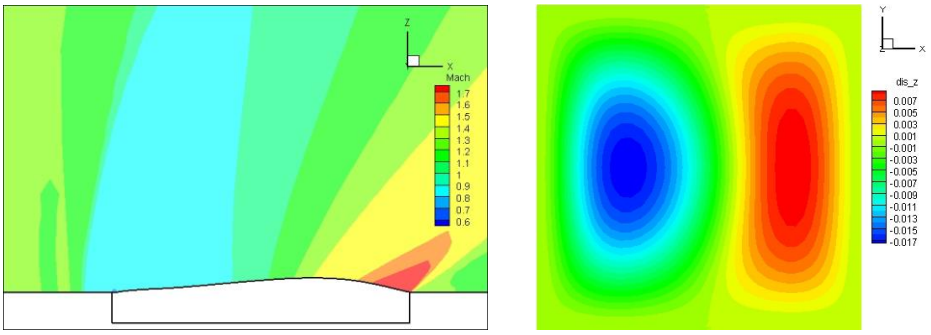

(a) Mach number distribution at the section y/b=0.5; (b) Displacement distribution of the panel

Fig. 4 Mach number and displacement distribution at λ=226 for Case 2

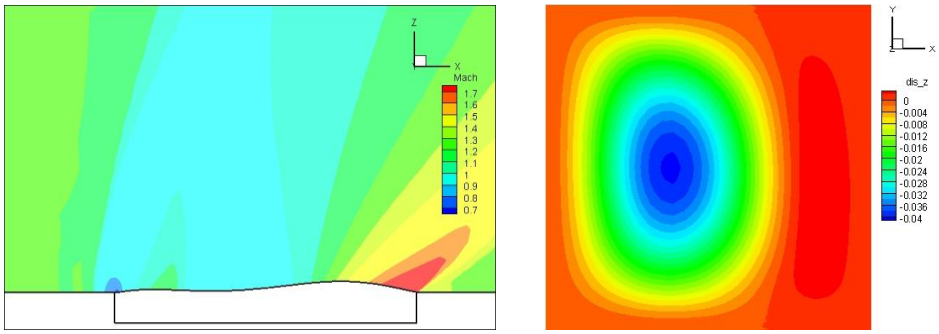

(a) Mach number distribution at the section y/b=0.5; (b) Displacement distribution of the panel

Fig. 5 Mach number and displacement distribution at λ=226 for Case 3

Fig. 6 shows the amplitudes of flutter onset and post-flutter oscillations. It can be found that with the increase of the dynamic pressure, the amplitude augments for cross-ply panels; on the contrary, the amplitude decreases for the angle-ply panel. Moreover, the critical dynamic pressure corresponding to the flutter onset of the angle-ply panel with R=2.5m is much higher than that of the other two cross-ply panels.

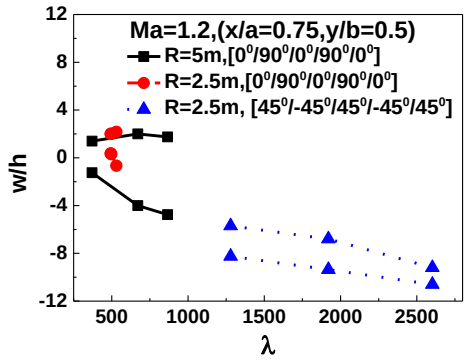

Fig. 6 Amplitude vs. dynamic pressure

For the Case 1 with *R*=5m and [0°/90°/0°/90°/0°], when λ=371, the time-histories of the displacement at the reference point present a profound change as seen in Figs. 7 (a)-(d). The trajectory can be divided by three stages: [0, 0.58s], [0.58s, 1.34s] and [1.34s, 1.67s]. At the first stage, the motions appear as chaotic form, with the time passing, they turn as non-period oscillations and finally, they tend to a limit cycle. Seen from Fig. 7(b) and Fig. 7(c), the oscillations at the second stage comprise the shape of the third one, besides, the four dominant frequency peaks being in ratio 1:2:3:4 as seen in Fig. 7(d). Figures 8 (a) and (b) show the displacement distribution in the z-direction at the time of positive and negative peaks of the limit cycle oscillation at the reference point, respectively. There are still two reverse peaks on the front and back part of the panel, respectively, and the displacement distribution are somewhat non-symmetrical about y/b=0.5 (as the oscillation contains some non-symmetrical modes of the structure).

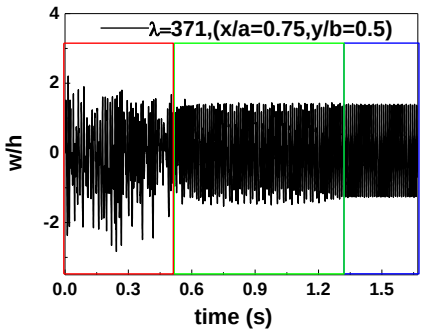

(a) Time-histories of the Oscillation;

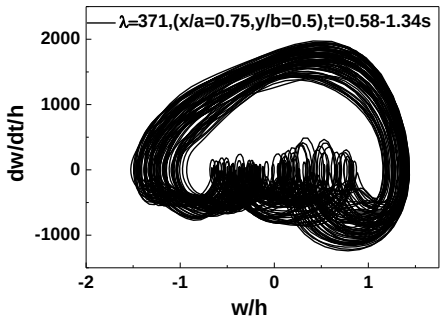

(b) Phase portrait at t=0.58-1.34s;

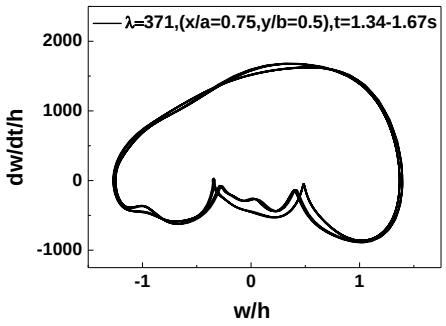

(c) Phase portrait at t=1.34-1.67s;

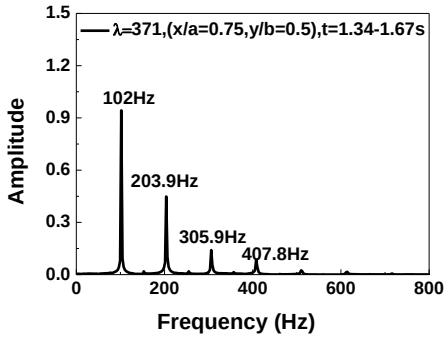

(d) Frequency Spectrum at t=1.34-1.67s

Fig. 7 Aeroelastic responses at λ=371 for Case 1

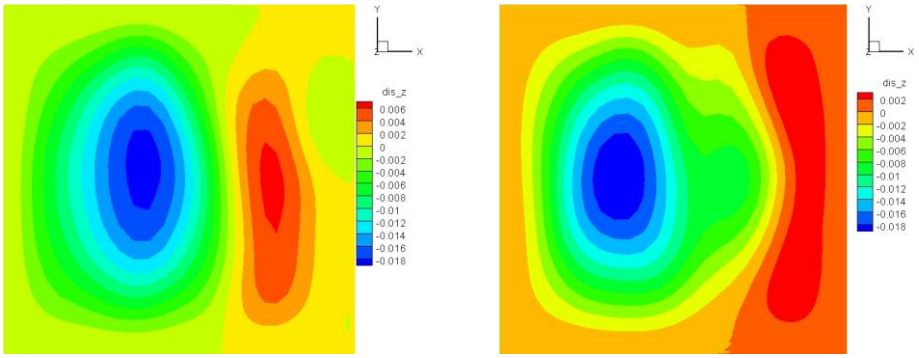

(a) t=1.508s, positive peak of the oscillation; (b) t=1.515s, negative peak of the oscillation

Fig. 8 Displacement distribution in the z-direction of the panel at λ=371 for Case 1

The same calculations conducted at λ=493 for Case 2 with R=2.5m and [0°/90°/0°/90°/0°] are shown in Figs. 9 - 11. The oscillations appear as a quasi-periodic pattern and the spectrum as shown in Fig. 9 (d) is regular with the ratio of the frequency peaks at near 1:2:3:4:5:6:7:8. Seen from the Mach number distribution in Figs. 10 (a) and 11(a), obviously, there exists a subsonic region behind the bow shock wave on the leading edge of the panel. Figures 10 (b) and 11(b) show the displacement distribution in the z-direction on the surface of the panel at the time of two points with maximum and minimum values of the oscillation.

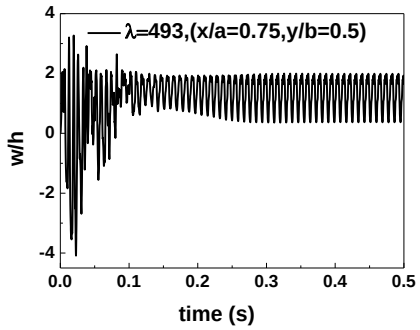

(a) Time-histories of the Oscillation;

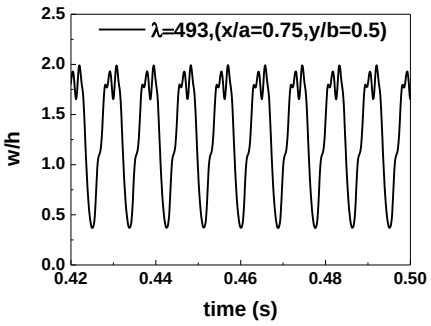

(b) The enlarged detail of the oscillation;

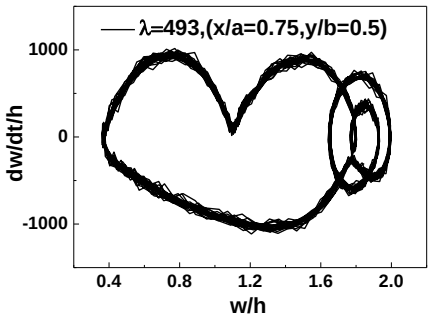

(c) Phase portrait;

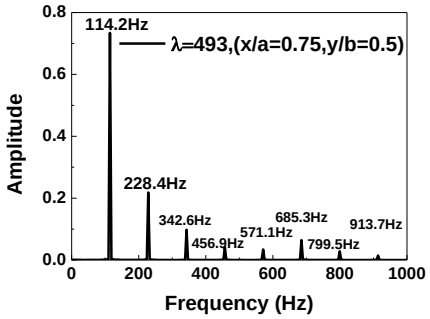

(d) Frequency Spectrum

Fig. 9 Aeroelastic responses at λ=493 for Case 2

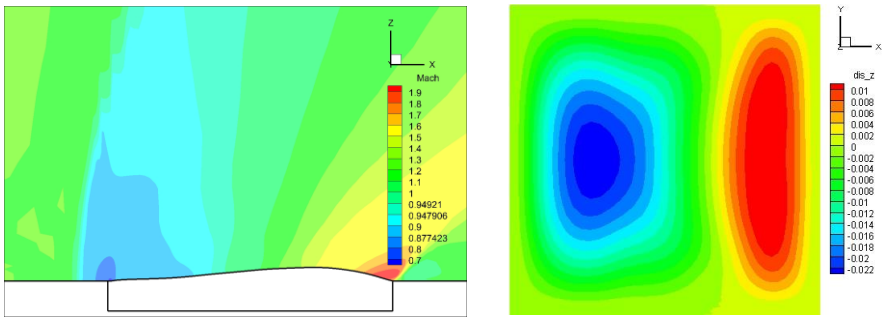

(a) Mach number distribution at the section y/b=0.5; (b) Displacement distribution of the panel

Fig. 10 Mach number and displacement distribution at t=0.422s under λ=493 for Case 2

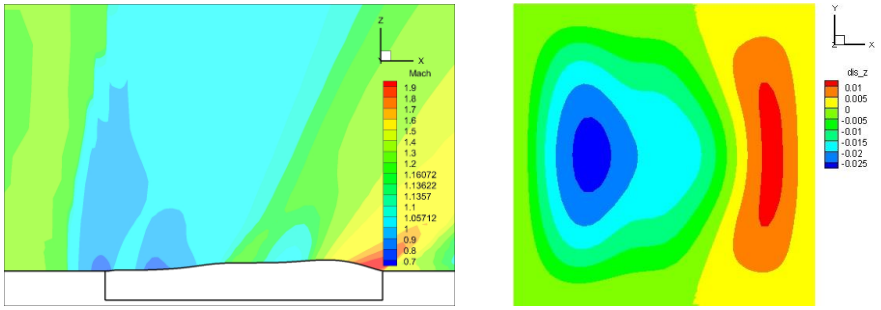

(a) Mach number distribution at the section y/b=0.5; (b) Displacement distribution of the panel

Fig. 11 Mach number and displacement distribution at t=0.425s under λ=493 for Case 2

For Case 3 with R=2.5m and [45°/-45°/45°/-45°/45°], the three different patterns of the oscillation occur when λ=1279 as seen in Fig. 12 at the respective stages: [0.08s, 0.3s], [0.4s, 0.8s] and [0.85s, 1.3s]. At the first stage, t=0.08-0.3s, the process presents as quasi-periodic form, and the amplitude of the oscillations increases with the passage of time as shown in Fig. 12 (b). Then at the initial steps of the second stage, t=0.4-0.8s, the trajectory appears as a pure limit cycle oscillation and the amplitude is higher than the previous one. However, after t=0.5s, the amplitude augments apparently, and the ratio of the dominant frequency peaks is almost 1:2:3:4:5:6. At t=0.85s, the oscillation switches to another quasi-periodic shape with constant amplitude cycles as seen in Fig. 12 (d). Note that the main frequency peaks of these cycles have nearly the same relation to those of the second stage, but the amplitudes of these frequency peaks are different. Figures 13 (a) and (b) show the displacement distribution in the z-direction on the surface of the panel at the time of the maximum point and the minimum point of the oscillation at the third stage, there exists only one negative peak during the oscillation.

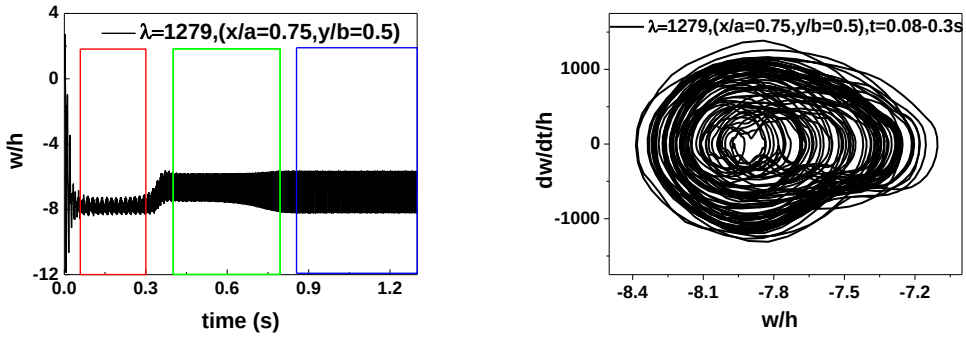

(a) Time-histories of the oscillation; (b) Phase portrait at t=0.08-0.3s;

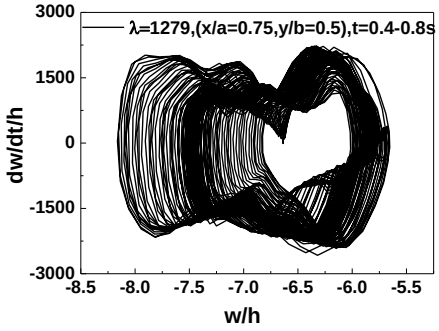

(c) Phase portrait at t=0.4-0.8s;

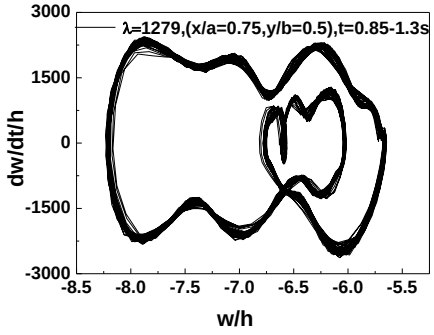

(d) Phase portrait at t=0.85-1.3s;

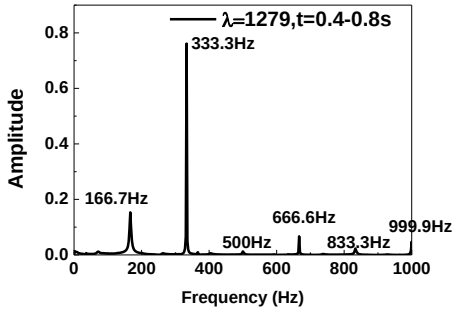

(e) Frequency spectrum at t=0.4-0.8s;

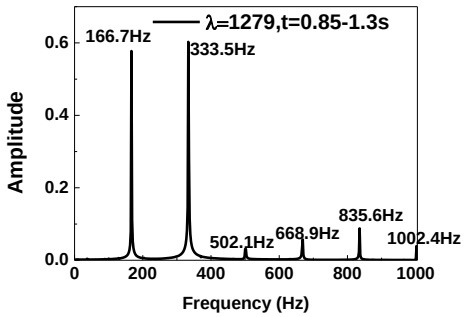

(f) Frequency spectrum at t=0.85-1.3s

Fig. 12 Aeroelastic responses at λ=1279 for Case 3

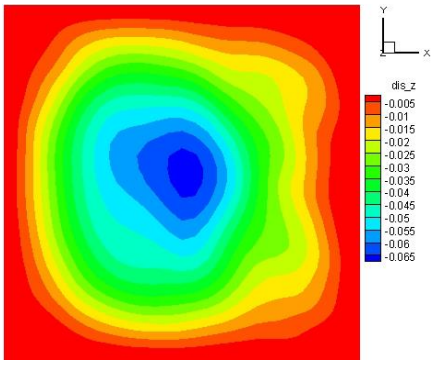

(a) t=1.0166s, maximum point of the oscillation;

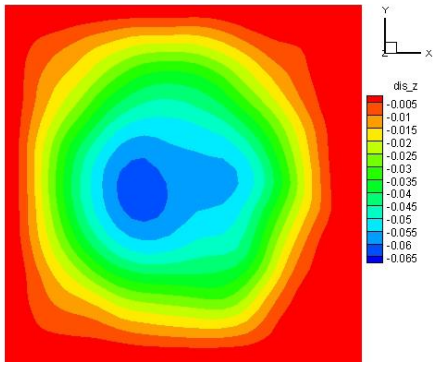

(b) t=1.04455s, minimum point of the oscillation

Fig. 13 Displacement distribution in the z-direction of the panel at λ=1279 for Case 3

4. Conclusions

Comparing with the other two cross-ply panels, the static aeroelastic deformation and the flutter dynamic pressure of the panel of angle-ply is the largest. The pattern of the oscillation of the panels of *R*=5m with [0°/90°/0°/90°/0°] and *R*=2.5m with [45°/-45°/45°/-45°/45°] can be described as under three different stages, and it takes a long period to capture the constant amplitude feature at Ma=1.2. Furthermore, for the panels with *R*=2.5m, the flow field presents a mixed flow containing both subsonic and supersonic regions; this means that the linearized aerodynamic algorithms, such as piston theory cannot be employed effectively.

References

- Journal article

1. Shiau, L.C., Lu, L.T.: Nonlinear flutter of composite laminated plates. Mathematical and Computer Modelling, 14, 983-988 (1990)
2. Ganapathi, M., Varadan, T. K., and Jijen, J.: Field-consistent element applied to flutter analysis of circular cylindrical shells. Journal of Sound and Vibration, 171, 509-527 (1994)
3. Singha M.K., Mandal M.: Supersonic flutter characteristics of composite cylindrical panels. Composite Structures, 82, 295-301 (2008)
4. Castro, S., Guimarães, T., Rade, D.: Flutter of stiffened composite panels considering the stiffener's base as a structural element. Composite Structures, 140, 36-43 (2016)
5. Jameson, A.: An assessment of dual-time stepping time spectral and artificial compressibility based numerical algorithms for unsteady flow with applications to flapping wings. AIAA 2009–4273 (2009)